frontiers | Frontiers in Mechanical Engineering

TYPE Original Research
PUBLISHED 18 December 2025
DOI 10.3389/fmech.2025.1727068

OPEN ACCESS

EDITED BY
Chengxi Zhang,
Jiangnan University, China

REVIEWED BY
Yu Yan,
Sun Yat-sen University, China
Peilin Jia,
Dalian University of Technology, China
Guangxin Guo,
Sun Yat-sen University, China

*CORRESPONDENCE
Jiwu Wang,
jiwuwang0505@163.com

RECEIVED 17 October 2025
REVISED 26 November 2025
ACCEPTED 01 December 2025
PUBLISHED 18 December 2025

CITATION
Wang J (2025) Life prediction of NC machine tools based on DT technology and LSTM technology.
Front. Mech. Eng. 11:1727068.
doi: 10.3389/fmech.2025.1727068

Life prediction of NC machine tools based on DT technology and LSTM technology

Jiwu Wang*

Department of Mechanical Engineering, Qinhuangdao Polytechnic Institute, Qinhuangdao, China

In order to solve the problems of physical model simplification error, insufficient fusion of multi-source monitoring data, and low accuracy of life prediction in traditional CNC machine tool life prediction methods, this study proposes a CNC machine tool remaining useful life (RUL) prediction method that combines digital twin (DT) technology with long short-term memory (LSTM) network. This study constructed a multi physics domain mapping model for CNC machine tools based on DT technology. A multimodal data preprocessing module was introduced into the DT model to extract key degradation features of the machine tool, and an improved LSTM network was developed. By inputting the high-dimensional degraded features output by the DT model into the LSTM network, accurate RUL prediction of CNC machine tools has been achieved. The results show that the proposed model performs well in all core indicators: during the accelerated degradation stage, the prediction accuracy is 96.1%, the average absolute error is only 8.9 h, and the maximum deviation is only 15 h, while maintaining a 100% physical constraint compliance rate and an effective prediction speed of 22 ms. In addition, as the proportion of the system increases, the indicators of the model rapidly improve; When the system proportion reaches 40%, the accuracy exceeds 40%, the recall rate approaches 42%, and the F0.5 score significantly improves. These findings indicate that the proposed method can effectively reduce equipment downtime losses, improve production efficiency, and provide a new technological approach for predictive maintenance of CNC machine tools.

KEYWORDS

digital twin, long short-term memory, numerical control machine tool, life prediction, maintenance

1 Introduction

As an essential component of high-end equipment manufacturing, the operational status of numerical control (NC) machine tools directly determines product processing accuracy and production efficiency (Hu et al., 2024). Traditional periodic maintenance models fail to effectively predict the remaining useful life (RUL) of components, often leading to issues of over-maintenance or under-maintenance. Therefore, achieving accurate RUL prediction for NC machine tools has become a research focus in the realm of intelligent manufacturing (Pantelidakis and Mykoniatis, 2024). In recent times, with the advancement of industrial internet technology, digital twin (DT) technology has introduced an innovative solution to bridge the gap between physical models and actual operating conditions—by constructing real-time mappings between physical entities and virtual models, DT enables dynamic perception and simulation of equipment states throughout their entire lifecycle. Meanwhile, long short-term memory (LSTM), a typical model in the

field of deep learning, offers unique advantages in processing long-term sequential degradation data, effectively capturing nonlinear characteristics during equipment degradation processes (Uribe et al., 2024).

Addressing the issue of model consistency challenges when applying DT technology to NC machine tools due to their complex structures and working conditions, Pei et al. proposed a four-layer modeling framework incorporating a requirement layer. They collected and processed multi-source data, developed real-time cutting algorithms, and validated model characteristics using methods such as the Fuzzy Analytic Hierarchy Process (FAHP). Additionally, they employed CNN-LSTM Attention to detect tool wear. The effectiveness of the framework was verified through a case study on an NC lathe, providing references for model construction and state detection in DT- and LSTM-based machine tool life prediction (Pei et al., 2025). To tackle the problem of insufficient modeling accuracy in traditional methods caused by the suboptimal matching between thermal error measurement points and predictive models in NC machine tools, Sa et al. introduced an integrated optimization approach for measurement point layout and error modeling under DT. Combining LSTM with dual-stage attention mechanisms and convolutional neural network (CNN)-based error modeling, the method achieved high-precision thermal error prediction, as demonstrated in experiments. When applied to grinding machine DT, it improved machining accuracy, offering insights into modeling and optimization for DT- and LSTM-based machine tool life prediction (Sa et al., 2024a). Addressing the high costs, excessive material consumption, and safety risks associated with servo system parameter design experiments on actual NC machine tools, Xie et al. utilized a programmable logic controller provided by Siemens, which integrated modeling, simulation, programming, debugging, and communication functions, to construct a DT experimental platform. Using a single-axis servo system as an example, they optimized parameters. The results showed that the platform reduced costs, enhanced parameter design accuracy and efficiency, and simulated real machine tool dynamics, providing ideas for LSTM-based life prediction of NC machine tools (Xie et al., 2024). To resolve the issue of smooth motion benefits disappearing due to servo drivers' inability to respond to differential characteristics in NC machine tools, along with machining contour errors influenced by servo errors, Kombarov et al. investigated the correlation between servo errors and interpolation acceleration. They established a predictive model based on experimental data and tested it on platforms such as DT models. The introduced acceleration and jerk FFW control approach was confirmed to compensate for differential characteristic impacts, offering error control references for DT- and LSTM-based machine tool life prediction research (Kombarov et al., 2025).

Tackling the challenge of swiftly constructing consistent multi-domain DT models for mechatronic equipment with electromechanical-hydraulic control coupling (e.g., NC machine tools), Wei Y et al. synthesized existing methods to propose multi-domain, multi-level DT models, along with construction guidelines and processes. They used Simscape to build a multi-domain DT model of an NC machine tool, verifying the feasibility of the approach and providing reliable model construction references for DT- and LSTM-based machine tool life prediction (Wei et al., 2024). In response to the lack of systematic development methods for DT in machine tool commissioning, despite the need to leverage DT to accelerate this process under advancing information technology, Norberger et al. conducted a systematic analysis of scientific publications in the DT field of NC production systems. Their aim was to identify systematic development methods and introduce new application progress, offering methodological references for DT construction and application in subsequent LSTM-based NC machine tool life prediction research (Norberger et al., 2024). To address the dynamic adjustment of maintenance and fault warning requirements in structural reliability assessments for reusable spacecraft mission planning, Gao et al. proposed a dynamic reliability prediction approach based on a DT framework. Using dynamic Bayesian networks to integrate uncertainty and update models, numerical case studies verified that the method could calibrate crack predictions, reduce uncertainty, and extend service life (Gao et al., 2023). To tackle the issue of machining accuracy being affected by dynamic and static errors in NC machine tools, along with the need for real-time machining quality estimation to achieve closed-loop control, Sa et al. proposed a DT synchronous evolution method that correlates these two types of errors. They constructed an intrinsic model incorporating static errors, collected multi-scenario data, and analyzed dynamic errors. Integrating the method into a DT platform validated its effectiveness, providing error correlation and data processing ideas for DT- and LSTM-based machine tool life prediction (Sa et al., 2024b).

In summary, regarding the life prediction of NC machine tools, existing research integrating DT technology with deep learning still faces limitations. DT models predominantly focus on geometric modeling and static performance simulation, lacking real-time mapping capabilities for the dynamic degradation processes of equipment and failing to incorporate life prediction functionalities. Additionally, the fusion of data-driven models and DT models merely utilizes monitoring data output by DT models as inputs, without achieving deep integration at the feature level. This results in models being unable to leverage DT's physical prior knowledge to correct prediction biases in data-driven models. Therefore, this study proposes a coupled framework integrating DT models with LSTM technology. First, a thermal-mechanical-vibration coupling model is embedded within the DT model, and a multimodal feature fusion algorithm based on an attention mechanism is designed to innovatively fuse physical simulation data output by the DT model with actual monitoring data at the feature level. Second, an improved LSTM prediction model is constructed by introducing gated recurrent units (GRUs) and attention mechanisms, optimizing the forget and input gate structures of LSTM to reduce noise interference in long-term sequential data. The research aims to support the formulation of predictive maintenance strategies, enabling life prediction and equipment operation and maintenance management.

The research is structured in the following way: The first section elaborates on the research background, significance, and prospects of life prediction for NC machine tools. The second section focuses on explaining the algorithm flow of the NC machine tool life prediction method designed in this study, which is based on DT models and LSTM technology. This section also constitutes the core focus and innovation of the research. The third section provides a

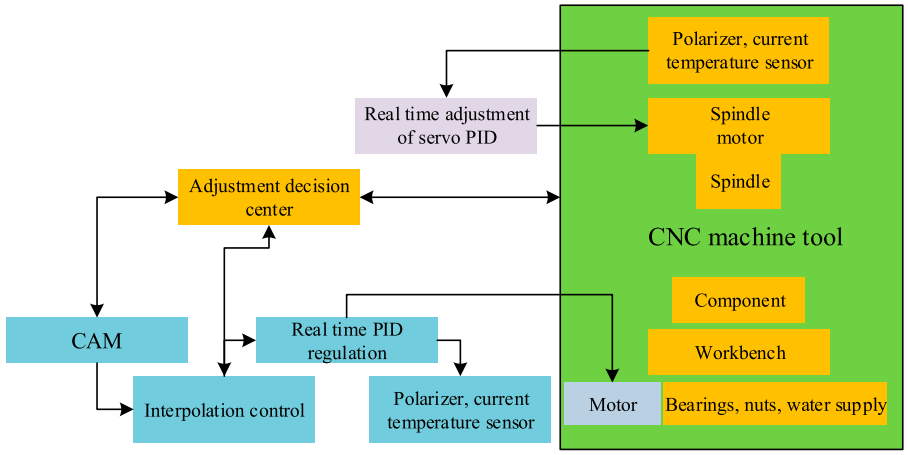

FIGURE 1
Physical model of traditional NC machine tools.

detailed analysis of experimental data results derived from the research methods outlined in the second section. The fourth section draws conclusions based on the experimental results, discussing the limitations of the current design and directions for further in-depth research in the future.

2 Methods and materials

The study proposes an approach for predicting the RUL of NC machine tools by integrating DT technology with LSTM networks. First, a multi-physics domain mapping model for NC machine tools is constructed based on DT technology. Second, a multi-modal data preprocessing module is innovatively embedded within the DT model. Finally, an improved LSTM network is developed, utilizing high-dimensional degradation features output by the DT model as inputs to achieve accurate RUL prediction for NC machine tools.

2.1 Construction of RUL model for NC machine tools based on DT

The degradation process of NC machine tools is the result of multi-physics field coupling effects. For instance, when the spindle rotates at high speeds, frictional heat is generated, leading to an increase in temperature and subsequent thermal deformation. This thermal deformation, in turn, alters the contact force between the spindle and the cutting tool, thereby exacerbating bearing wear and degradation (Wang et al., 2024; Peterson et al., 2025). Traditional physical models typically simplify this process using a "single-field modeling + linear superposition" approach, which fails to accurately reflect the impact of multi-field coupling on equipment degradation. Meanwhile, purely data-driven models lack constraints from physical prior knowledge, making them prone to discrepancies between predicted results and actual degradation patterns when monitoring data contains noise or is incomplete (Tao et al., 2024). The traditional physical model of NC machine tools is illustrated in Figure 1.

In Figure 1, traditional physical models and purely data-driven models, lacking physical prior constraints, are prone to prediction results that deviate from actual degradation patterns when encountering noisy or incomplete monitoring data, failing to adequately meet the demands of equipment state analysis under complex operating conditions. The complex structure of NC machine tools, featuring multi-component collaboration and multi-sensor monitoring as depicted in Figure 1, also indirectly demonstrates the difficulty traditional methods face in comprehensively and accurately characterizing their degradation processes.

Based on this, the study constructs a DT model for NC machine tools, achieving dynamic mapping between the physical entity and virtual model, as well as degradation state perception, through the following three core modules: (1) a numerical simulation model incorporating thermal-mechanical-vibration coupling; (2) a real-time data synchronization module enabling 10 Hz-level data interaction between the physical equipment and virtual model via industrial Ethernet; and (3) a degradation state assessment module that extracts key degradation indicators of the equipment based on multi-physics field simulation results.

The specific steps for researching and implementing multi physics field coupling simulation are as follows: Firstly, geometric modeling: Three-dimensional geometric model of the spindle bearing guide rail is established, and tetrahedral elements are used for mesh division; Secondly, multi field coupling setup: The thermal field module adopts a 'solid heat transfer' physical field, introduces the heat conduction equation and boundary conditions, and real-time calls temperature sensor data to update the environmental temperature boundary; The force field module adopts the physical field of 'structural mechanics', based on Hertz contact theory and thermal stress calculation equation, and takes the cutting force collected by the piezoelectric force gauge as the external load input; The vibration field module adopts the physical field of 'acoustic structural interaction', and combines the temperature distribution calculated by the vibration equation with the stress distribution calculated by the force field to achieve bidirectional coupling of the three fields of heat force vibration.

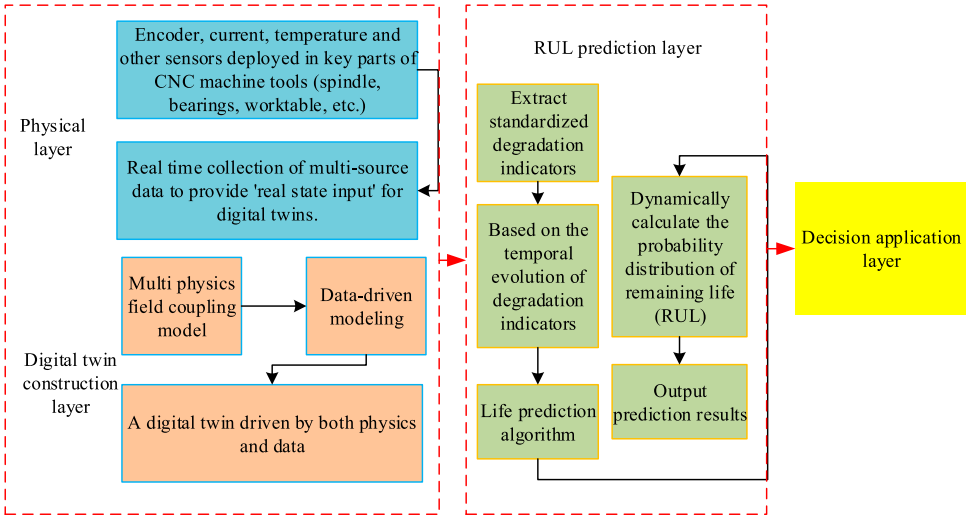

FIGURE 2
DT model of NC machine tool.

This DT model not only provides more accurate degradation process simulation than traditional physical models but also supplies physical constraints for subsequent LSTM prediction models, avoiding the "data-driven black box" issue (Zohdi, , 2025). The DT model of the NC machine tool is illustrated in Figure 2.

In Figure 2, the multi-physics domain coupling model is first divided into a thermal field model, a mechanical field model, and a thermal-mechanical-vibration coupling model. The thermal field distribution of the spindle system in NC machine tools adheres to Fourier's law of heat conduction, accounting for frictional heat generated by spindle rotation, cutting heat, and convective heat dissipation. Its three-dimensional unsteady-state heat conduction process is presented in Equation 1.

$$\rho c \frac{\partial T}{\partial t} = \nabla \cdot (k \nabla T) + q_v \tag{1}$$

In Equation 1, ρ is the density of the spindle material (kg/m^3), c is the specific heat capacity of the spindle material (J/(kg·K)), and T is the temperature field distribution (K); t is time (s); k is the thermal conductivity of the material (W/(m·K)); q_v is the intensity of the internal heat source (W/m^3), mainly including the frictional heat q_{v1} of the bearing and the loss heat q_{v2} of the spindle motor, that is, $q_v = q_{v1} + q_{v2}$. The calculation of the frictional heat q_{v1} of the bearing is based on the Palmgren formula, considering the effects of radial load F_r, axial load F_a, and rotational speed n, as shown in Equation 2.

$$q_{v1} = \frac{10^{-3} P_0 n}{V} \tag{2}$$

In Equation 2, P_0 is the total friction power of the bearing (kW), and f_0 is the friction coefficient; V is the volume of the bearing (m^3); n is the spindle speed (r/min). The thermal loss q_{v2} of the spindle motor is composed of copper loss, iron loss, and mechanical loss, as shown in Equation 3.

$$q_{v2} = \frac{P_{in}(1-\eta)}{V_m} \tag{3}$$

In Equation 3, P_{in} is the input power of the motor (kW), which is collected in real-time through a current sensor; η is the motor efficiency; V_m is the volume of the motor stator (m^3). The boundary conditions of the thermal field model include convective heat dissipation boundary and adiabatic boundary, as shown in Equation 4.

$$\begin{cases} -k\dfrac{\partial T}{\partial \boldsymbol{n}} = h(T - T_0) \\ \dfrac{\partial T}{\partial \boldsymbol{n}} = 0 \end{cases} \tag{4}$$

In Equation 4, h is the convective heat transfer coefficient (W/(m^2·K)); T T_0 is the ambient temperature (K), collected in real-time through a temperature sensor; $\boldsymbol{n}$ is the direction of the boundary normal vector. The force field of the spindle system mainly includes cutting force and bearing support force. Based on Hertz contact theory, the contact stress σ_H between the ball and the raceway is presented in Equation 5.

$$\sigma_H = 0.418\sqrt{\frac{F_z E}{R_{eq} b}} \tag{5}$$

In Equation 5, F_z is the axial cutting force (N), which is collected in real-time by a piezoelectric force gauge; E is the equivalent modulus of elasticity (Pa); R_{eq} is the equivalent curvature radius (m), $R_{eq} = \frac{R_1 R_2}{R_1 + R_2}$, R_1 is the ball radius, and R_2 is the raceway curvature radius; b is the contact width (m), $b = 2\sqrt{\frac{2F_z R_{eq}}{\pi E L}}$, and L is the effective contact length of the bearing (m). The influence of cutting force on spindle deformation is solved using finite element method. Based on the principle of virtual work, the static equilibrium equation of the spindle is presented in Equation 6.

$$\mathbf{K\delta} = \mathbf{F} \tag{6}$$

In Equation 6, $\mathbf{K}$ is the stiffness matrix of the main axis (N/m), which is obtained through modal analysis using ANSYS software; $\boldsymbol{\delta}$

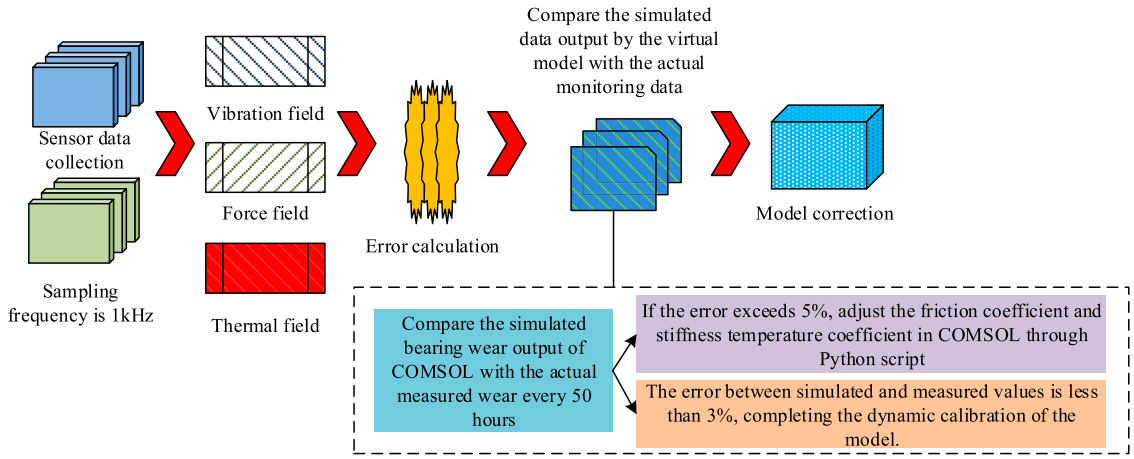

FIGURE 3
Dynamic update of DT model.

is the displacement vector of the main axis (m); **F** is the external force vector (N), including cutting force F_c, gravity G, and bearing preload F_p. The coupling between the thermal field and the force field is achieved through thermal stress caused by temperature, and the calculation of thermal stress σ_T is presented in Equation 7.

$$\sigma_T = \alpha E \Delta T \tag{7}$$

In Equation 7, α is the thermal expansion coefficient (1/K) of the spindle material; ΔT is the temperature change (K), i.e., $\Delta T = T - T_0$. The vibration field model is based on the dynamic characteristics of the spindle after thermal mechanical coupling, as shown in Equation 8.

$$\mathbf{M}\ddot{x} + \mathbf{C}\dot{x} + \mathbf{K}(T)x = \mathbf{F}(t) \tag{8}$$

In Equation 8, **M** is the mass matrix of the spindle system (kg); **C** is the damping matrix (N·s/m), using the Rayleigh damping model, $C = \alpha_M M + \beta_K K$; $\mathbf{K}(T)$ is the stiffness matrix (N/m) that varies with temperature, $\mathbf{K}(T) = \mathbf{K}_0(1 + \gamma \Delta T)$, K_0 is the stiffness matrix at room temperature, and γ is the temperature coefficient of stiffness; x, $\dot{x}$, and $\ddot{x}$ are the vibration displacement, velocity, and acceleration vectors (m, m/s, m/s^2), respectively; $\mathbf{F}(t)$ is the dynamic excitation force vector (N), including cutting force fluctuations and bearing unbalance forces (Qu et al., 2025). This study is based on a multi physics domain coupling model, defining key degradation indicators for NC machine tools, including: bearing wear amount W, calculated based on the Archard wear model; The thermal deformation of the spindle, δ_T, is calculated based on the thermal expansion formula; The effective value of vibration RMS is calculated based on the vibration acceleration signal. The above is presented in Equation 9.

$$\begin{cases} W = k_a \dfrac{F_N v t}{H} \\ \delta_T = L \alpha \Delta T \\ RMS = \sqrt{\dfrac{1}{N}\sum_{i=1}^{N} a_i^2} \end{cases} \tag{9}$$

In Equation 9, k_a is the wear coefficient, F_N is the normal contact force (N), v is the sliding velocity (m/s), t is the operating time (s), and H is the material hardness (HV); L is the effective length of the spindle (m); a_i is the i th vibration acceleration sampling value (m/s^2), and N is the number of sampling points. The dynamic update of the DT model is achieved through a closed-loop process of "data collection error compensation model correction", as shown in Figure 3.

As shown in Figure 3, after preprocessing, the multimodal degradation indicators output by the DT model are employed as input features for the LSTM model, tackling the challenge of singular feature extraction in traditional data-driven models. Additionally, the multi-physics domain coupling relationships within the DT model serve as regularization terms for the LSTM model, preventing physically implausible prediction results. Using a closed-loop process of 'data collection error compensation model update', the bearing wear output from COMSOL simulation is compared with the actual measured wear every 50 h (measured using a laser displacement sensor KEYENCE LK-G80 with an accuracy of ±0.1 μm). If the error exceeds 5%, the friction coefficient and stiffness temperature coefficient in COMSOL are adjusted through Python scripts until the error between the simulation value and the measured value is less than 3%, completing the dynamic correction of the model.

2.2 Life prediction of NC machine tools integrating DT and LSTM

Although the DT model can provide accurate degradation state assessments, it cannot directly predict the future RUL—this is because the degradation process of equipment exhibits characteristics such as nonlinearity and randomness, necessitating the use of data-driven models to capture these complex patterns (Information et al., 2024; Dimic et al., 2024). The traditional LSTM model has the following deficiencies when processing long-term sequential degradation data: unreasonable weight allocation for

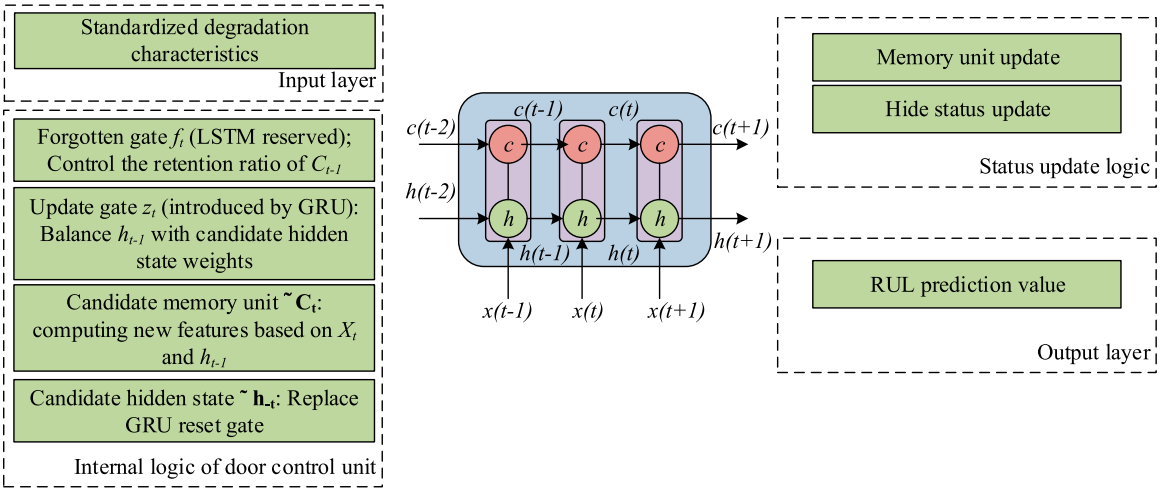

FIGURE 4
The interaction relationship between the core gating units of LSTM-GRU structure.

multimodal data, making it susceptible to interference from redundant features; noise in long-term sequential data can lead to gradient vanishing in the model, affecting prediction accuracy; and the lack of physical constraints may result in outputs that do not align with the actual degradation mechanisms. Therefore, by integrating DT technology with LSTM, a DT-LSTM life model for NC machine tools has been proposed, centered around a three-tier architecture of "feature fusion-sequential prediction-physical constraints": first, weight allocation for DT multimodal features is achieved through an attention mechanism; then, an improved LSTM network is constructed to capture sequential degradation patterns; finally, a physical constraint regularization term is introduced to optimize the prediction results.

To solve the problem of uneven weight allocation of multimodal features (wear, thermal deformation, vibration) in DT output, spatial attention mechanism is introduced (Kibira et al., 2024). Let the feature matrix output by DT be $\mathbf{X} = [DI_W, DI_{\delta_T}, DI_{RMS_a}] \in \mathbb{R}^{T\times D}$ (T is the time step, D = 3 is the feature dimension), and the attention weight α is calculated as shown in Equation 10.

$$\begin{cases} M = \tanh(\mathbf{W}_1 X + b_1) \\ \alpha = \mathrm{softmax}(\mathbf{W}_2 M + b_2) \end{cases} \tag{10}$$

In Equation 10, $\mathbf{W}_1 \in \mathbb{R}^{D\times D}, \mathbf{W}_2 \in \mathbb{R}^{D\times D}$ are the weight matrices, b_1 and b_2 are bias vectors, and $\alpha \in \mathbb{R}^{T\times D}$ is the attention weight, satisfying $\sum_{d=1}^{D} \alpha_{t,d} = 1$. The fused feature vector $\mathbf{X}_{att} \in \mathbb{R}^{T\times D}$ focuses on key degraded features (such as wear), as presented in Equation 11.

$$X_{att,t,d} = \alpha_{t,d} \cdot X_{t,d} \tag{11}$$

In Equation 11, $X_{att,t,d}$ is the fusion value of the t th time step and the d th dimensional feature.

To address the gradient vanishing problem in traditional LSTM models, the update gate mechanism of GRU is introduced while retaining the forget gate functionality of LSTM, thereby constructing a hybrid LSTM-GRU structure, as specifically illustrated in Figure 4.

In the hybrid LSTM-GRU architecture studied, LSTM controls information flow through forget gates, input gates, and output gates, and is good at capturing long sequence dependencies, but lacks stability in long-term gradient propagation; GRU is simplified into update and reset gates, with fewer parameters and higher training efficiency. The update gate can dynamically balance the weight of historical and current information. The degradation data of CNC machine tools is a 1800 h long sequence (36 time steps), which has the problem of early weak features being easily lost and mid-term gradients being easily attenuated. The hybrid architecture combines the advantages of both: the forget gate of LSTM preserves key historical degradation features (such as small changes in initial stage vibrations), while the update gate of GRU dynamically adjusts the information fusion ratio to avoid gradient vanishing caused by too small gradient products. Theoretically, it is more suitable for long sequence nonlinear degradation data than a single LSTM/GRU. The theoretical basis for solving the gradient vanishing problem with this hybrid structure is that traditional LSTM controls the retention of historical information through a forget gate. However, when processing 1800 h long sequence degraded data of machine tools, as the time step increases, the weight of the forget gate tends to accumulate and approach 0, resulting in the loss of early key degraded information (such as small vibration changes in the initial stage); The update gate of GRU can dynamically adjust the fusion weight of historical information and current information, complementing the LSTM forget gate. When the weight of the LSTM forget gate is too low, the GRU update gate can enhance the retention of historical information and avoid gradient loss due to too small weight product during backpropagation. In addition, the attention mechanism assigns weights to multimodal features (wear, thermal deformation, vibration) to focus the model on vibration features that are more sensitive to degradation, further reducing the interference of irrelevant features on gradient calculation. The steps of attention mechanism is clarified as follows: set the feature matrix output by DT, and calculate the attention mechanism steps: ① Feature mapping: map the feature

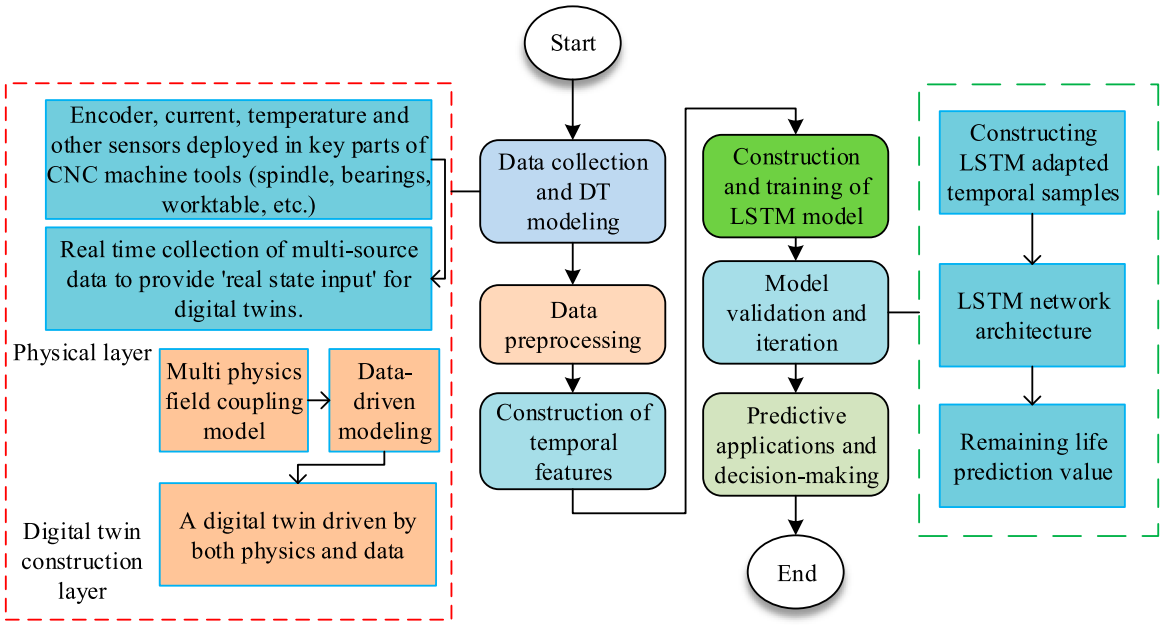

FIGURE 5
Life prediction process of NC machine tool combining DT and LSTM technology.

matrix output by DT to intermediate features through the weight matrix; ② Weight calculation: Compress intermediate features into one-dimensional attention weights through a weight matrix; ③ Feature fusion: Weighted fusion of features in the time step dimension, focusing on time step features that are more sensitive to degradation. As shown in Figure 4, the calculations of forget gate f_t, update gate z_t, candidate memory unit $\tilde{C}_t$, and output gate o_t are presented in Equation 12.

$$\begin{cases} f_t = \sigma\left(\mathbf{W}_f\left[h_{t-1}, X_{att,t}\right] + b_f\right) \\ z_t = \sigma\left(\mathbf{W}_z\left[h_{t-1}, X_{att,t}\right] + b_z\right) \\ \tilde{C}_t = \tanh\left(\mathbf{W}_c\left[h_{t-1}, X_{att,t}\right] + b_c\right) \\ C_t = f_t \odot C_{t-1} + (1 - z_t) \odot \tilde{C}_t \end{cases} \tag{12}$$

In Equation 12, σ is the Sigmoid activation function, $\odot$ is the product of elements, h_{t-1} is the previous hidden state, C_{t-1} is the previous memory unit, and $\mathbf{W}_f$、$\mathbf{W}_z$、$\mathbf{W}_c$ are the weight matrices. The hidden state h_t and the final RUL prediction value $\hat{y}_t$ are presented in Equation 13.

$$\begin{cases} o_t = \sigma\left(\mathbf{W}_o\left[h_{t-1}, X_{att,t}\right] + b_o\right) \\ h_t = o_t \odot \tanh\left(C_t\right) \\ \hat{y}_t = \mathbf{W}_y h_t + b_y \end{cases} \tag{13}$$

In Equation 13, $\mathbf{W}_o, \mathbf{W}_y$ are the weight matrices, and $\hat{y}_t$ is the RUL prediction value (h) at the t th time step. To avoid predicting results that violate physical laws (such as negative RUL and excessive wear), a physical constraint term R is introduced to optimize the loss function, as shown in Equation 14.

$$R = \lambda_1 \max\left(0, W_{pred} - W_{max}\right) + \lambda_2 \max\left(0, \sigma_{pred} - \sigma_{max}\right) \tag{14}$$

In Equation 14, W_{pred} and σ_{pred} are the wear and stress values predicted by LSTM, and λ_1 and λ_2 are the constraint weights (Preethi and Mamatha, 2023). The integration of physical constraint forms and loss functions is clarified as follows: Physical constraints are based on the basic laws of CNC machine tool operation, and define two hard constraints: ① Wear amount constraint: predicted wear amount ≤ maximum wear amount; ② Stress constraint: predicted stress ≤ yield strength); The design of the physical constraint regularization term is: L_phy = lambda$_1$ x max (0, W_pred - W_max)+lambda$_2$ x max (0, σ _pred - σ _2), where lambda$_1$ = 10 and lambda$_2$ = 5 (determined through cross validation to balance prediction error and constraint compliance); The total loss function integrates MSE with physical constraints: L_total = MSE (y_true, y_pred)+L_phy, where MSE (y_true, y_pred) is the mean square error between the predicted RUL and the true RUL, y_true is the measured RUL, and y_pred is the model predicted RUL.

Using Mean Squared Error (MSE) combined with physical constraints, the total loss function L is presented in Equation 15.

$$L = \frac{1}{N}\sum_{t=1}^{N}\left(y_t - \hat{y}_t\right)^2 + R \tag{15}$$

In Equation 15, y_t is the actual RUL value (h), and N is the number of samples. Based on the above research, the life prediction process of NC machine tools using DT and LSTM technologies is presented in Figure 5.

As shown in Figure 5, at the physical layer, multi-source data is collected through sensors, and a "physical + data" dual-driven DT is constructed via the DT construction layer to accomplish data acquisition and DT modeling. Subsequently, the data is processed to construct sequential features. Then, the process moves to the LSTM model phase, where an LSTM model is established and trained, followed by iterative validation and optimization to achieve predictive applications and decision-making, clearly

demonstrating the complete workflow from data acquisition to life prediction applications.

The integration core of DT model and LSTM network is the closed-loop coupling of "physical simulation feature extraction → multimodal feature fusion → temporal prediction → physical constraint optimization". The specific workflow and data flow are as follows: DT model feature output stage: based on the constructed "thermal mechanical vibration" multi physics field coupling DT model, output one set of standardized degradation features every 50 h, and output the physical credibility score of each feature. Feature preprocessing and fusion stage: Data cleaning removes abnormal features with a credibility<0.6 from DT output, and uses linear interpolation to fill in missing data; Attention feature fusion: By using spatial attention mechanism, weights are assigned to the cleaned 3D features, and a 1D temporal feature vector is generated after fusion. LSTM temporal prediction stage: The fused feature vectors are divided into a training set in a 7:3 ratio and input into an improved LSTM network (LSTM-GRU hybrid structure). Training process: After each round of training, the LSTM outputs the predicted RUL and physical constraint terms. If the predicted value violates physical laws, a loss function penalty is triggered, and the network weights are adjusted by backpropagation; Feedback correction: Every 100 h, the RUL value predicted by LSTM is fed back to the DT model to update the degradation trend simulation parameters of DT, so that the features output by DT in the next round are more in line with the actual degradation law.

The interface details between DT and LSTM are as follows: ① Data transmission format: The DT model completes a multi physics field simulation every 50 h, outputs standardized degradation features and feature reliability scores (0–1), and stores them in the MySQL 8.0 database; ② Data reading: LSTM reads database data at regular intervals (every 50 h) through Python's pandas library (version 2.1.0), filters out abnormal features with a credibility<0.6, and uses linear interpolation to fill missing values (missing rate ≤0.5%); ③ Data preprocessing: Perform Min Max normalization on the read features (normalization range [0,1]); ④ Feedback mechanism: LSTM feeds back the predicted RUL to the DT model every 100 h to update the degradation trend simulation parameters of DT. The algorithm pseudocode is as follows.

```
Input: Physical equipment sensor data (temperature, vibration, force, current), material parameters, equipment rated parameters
Output: RUL prediction value of CNC machine tool (h)
1. Initialize DT model
  1.1 Build a three-dimensional geometric model (spindle, bearings, guide rails) with a mesh resolution of 0.1 mm (tetrahedral elements)
  1.2 Configure multiple physical field parameters:
    - Thermal field: k = 51 W/(m · K), C = 465 J/(kg · K), residual threshold 1e-6
    - Force field: E = 208 GPa, μ = 0.3, residual threshold 1e-6
    - Vibration field: Rayleigh damping (α = 0.01, β = 0.001), residual threshold 1e-6
  1.3 Embedded multimodal data preprocessing module (denoising, normalization, credibility rating)
2. Dynamically update DT model and extract features
  While the device is running:
  2.1 Collecting Sensor Data (Sampling Frequency: Temperature/Current 1 Hz, Vibration 1 kHz, Force 100 Hz)
  2.2 Synchronize to DT virtual model and perform multi physics field coupling simulation (up to 500 iterations)
  2.3 Extract standardized degradation features X = [W, δ _T, RMS], calculate reliability score
  2.4 If score ≥0.6: Store X in the database; Otherwise: discard the set of features
  2.5 Every 100 h: Receive RUL prediction values from LSTM feedback and correct DT simulation parameters
  2.6 When the cumulative number of features is ≥36 (corresponding to 1800 h): proceed to step 3
3. Attention mechanism feature fusion
  3.1 Read 36 sets of features from the database and construct a feature matrix X ∈ R^(36 × 3)
  3.2 Calculate attention weight α = softmax (W 2× tanh (W 1× X^T + b 1)+b 2)
  3.3 Weighted fusion yields X_att ∈ R^(1 × 3)
4. Training a Hybrid LSTM-GRU Model
  4.1 Divide the dataset into 70% training set, 15% validation set, and 15% test set
  4.2 Initialize model hyperparameters: Learning rate 0.001, batch size = 32, epochs = 200
  4.3 Definition of loss function: L_total = MSE (y_true, y_pred)+lambda 1 x max (0, W_pre-W_max)+lambda 2 x max (0, σ _pred - σ _2)
  4.4 Train the model using Adam optimizer and enable early stop strategy (patience = 20)
5. RUL prediction and output
  5.1 Input X_att into the trained model to obtain the RUL prediction value y_pred
  5.2 Verify whether y_pred satisfies physical constraints (W_pred ≤0.1 mm, σ _pred ≤835 MPa)
  5.3 If satisfied: output y_pred; Otherwise: trigger loss function penalty and re predict
```

Algorithm 1. RUL prediction algorithm for CNC machine tools based on DT-LSTM.

3 Results

To confirm the validity of the approach introduced in the research, an experiment was specifically conducted for this purpose. The design parameters and experimental data were examined to validate the benefits and practicality of the proposed method.

3.1 Performance analysis of the life prediction model for NC machine tools

Sensors were deployed on a vertical machining center during the experiment (two PT100 temperature sensors were attached to the spindle bearing housing, two PCB352C33 vibration sensors were fixed to the front end of the spindle and the

TABLE 1 Experimental hardware configuration.

Experimental dimension	Configuration	Specific parameters
Experimental subject	NC machine tool model	Vertical machining center VMC850
	Operating conditions	Spindle speed: 1,000–8,000 r/min; cutting load: 500–2000 N; experimental period: 1800 h
Monitoring system	Sensor type and quantity	Temperature sensor (PT100, 2 channels), vibration sensor (PCB 352C33, 2 channels), force sensor (Kistler 9257B, 1 channel), current sensor (LEM LA55-P, 1 channel)
Software tool	Data acquisition software	NI LabVIEW 2023
	DT simulation software	COMSOL Multiphysics 6.2+Python 3.9 (data interface)
	Deep learning framework	PyTorch 2.0 + CUDA 12.1
	Data management tools	MySQL 8.0
Computing hardware		CPU: Intel Xeon Gold 6,338 (28 cores); GPU: NVIDIA A100(40 GB VRAM); memory: 128 GB DDR4

feed guide rail, one Kistler 9257B force sensor was installed on the workbench, and one LEM LA55-P current sensor was connected in series to the power supply circuit of the spindle motor). The sensors were connected to an industrial computer via an NI cDAQ-9178 data acquisition card, and a 1000Mbps Ethernet network was established using an industrial switch to facilitate data exchange between devices. The DT simulation server (NVIDIA A100) and the LSTM training server (RTX 4090) were debugged, and it was confirmed that the GPU computing power was functioning normally (with computing power test values reaching ≥90% of the theoretical value under the CUDA 12.1 environment). The experimental configuration is detailed in Table 1.

The key details of the DT model are as follows. Mesh division details: The three-dimensional geometric model of the spindle, bearings, and guide rails is divided into tetrahedral elements, with a mesh resolution of 0.1 mm; the mesh quality inspection pass rate is ≥95%, and the distortion rate is ≤5%. Multi physics field coupling convergence criterion: The residual convergence threshold for thermal field, force field, and vibration field is set to 1e-6, and the upper limit of iteration is 500 times; The boundary conditions of the thermal field and force field are updated synchronously every 100 iterations. Parameter selection criteria: ① Material parameters: The spindle material is 40CrNiMoA, with a thermal conductivity of 51W/(m · K) and a specific heat capacity of 465J/(kg · K); the bearing material is GCr15, with an elastic modulus of 208 GPa and a Poisson's ratio of 0.3; ② Friction coefficient: The rolling friction coefficient of the bearing is 0.0012, and a correction coefficient (f_0 (T) = f_0× (1 + 0.002 Δ T)) is introduced considering the influence of temperature; ③ Heat source intensity: The proportion of copper and iron losses in the spindle motor is determined based on motor efficiency testing experiments.

The hyperparameter settings for the research model are as follows: The hyperparameters for model training are determined through grid search, as follows: ① Optimizer: Adam optimizer, β_1 = 0.9, β_2 = 0.999, ε = 1e-8; ② Learning rate: Initial learning rate of 0.001, using cosine annealing strategy (Tmax = 50, eta-min = 1e-5); ③ Batch size: 32; ④ Training epochs: 200; ⑤ Early Stopping Strategy: Monitor the MSE of the validation set, stop training if there is no decrease for 20 consecutive rounds, and restore the optimal weights; ⑥ Regularization: Weight decay = 1e-4 to suppress overfitting.

Operating conditions were set as follows: A spindle speed gradient and a cutting load gradient were established, with the feed rate fixed at 1,000 mm/min, the ambient temperature controlled at 25 ± 2 C, and an experimental duration of 1815 h. Standardized degradation indicators were recorded every 50 h. For dataset planning, the data was divided into a training set (1,275 h, encompassing full operating condition data) and a test set (540 h, matching high-frequency operating conditions in actual production: 6,000 r/min, 1500 N) at a ratio of 7:3. A 5-fold cross-validation method was employed to prevent model overfitting. For real-time data acquisition, the NI LabVIEW 2023 software was used to control sensor data collection, with sampling frequencies set at 1 Hz for temperature/current, 1 kHz for vibration, and 100 Hz for force. The data was stored in a MySQL 8.0 database, and a data backup (including both raw and preprocessed data) was generated every hour. Data preprocessing involved denoising (wavelet threshold denoising for vibration signals and moving average filtering for temperature signals) and filling in missing values (using linear interpolation for missing rates ≤0.5%), providing clean input data for the DT model.

Figure 6 presents a comparison of the algorithm running times under different confidence levels and support degrees. In Figure 6a, under varying confidence levels, the PSO-SVM algorithm generally exhibited the longest running times, mostly ranging from 80 to 100 m. The traditional LSTM algorithm followed, with running times approximately between 40 and 70 m, while the improved DT-LSTM algorithm had the shortest running times, mostly between 20 and 40 m. This indicated a significant efficiency advantage of the improved algorithm. In Figure 6b, under different support degrees, the PSO-SVM algorithm took the longest time, often exceeding 3,000 m, while the traditional LSTM algorithm had running times around 2000–4,000 m. The improved DT-LSTM algorithm again showed the shortest running times, mostly between 1,000 and

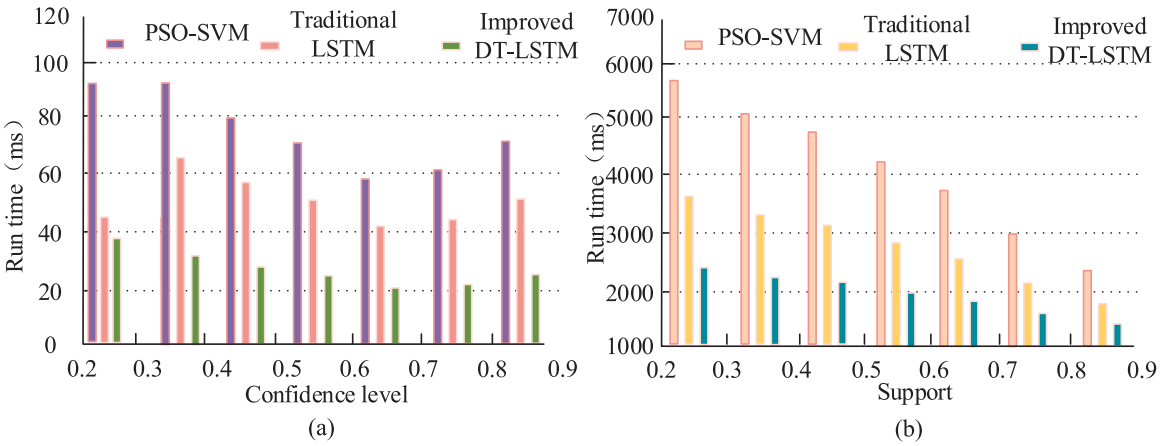

FIGURE 6
Comparison of algorithm running time under different confidence and support levels. **(a)** Running time of each algorithm at different confidence levels. **(b)** The running time of each algorithm under different support levels.

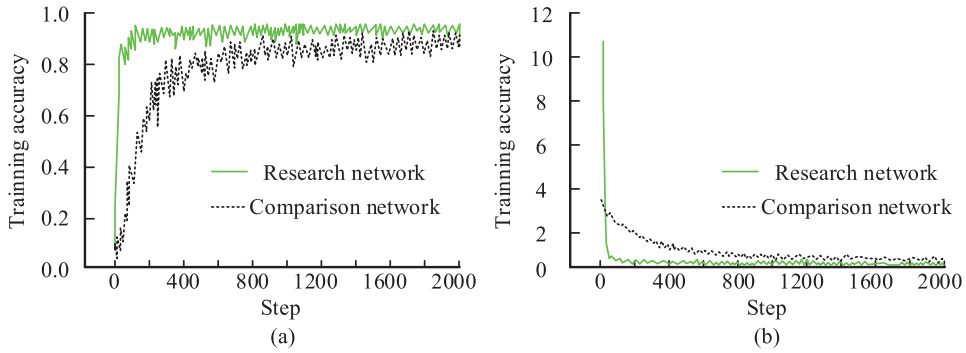

FIGURE 7
The training accuracy curve of the studied LSTM and traditional CNN. **(a)** Accuracy curves of models trained on various networks. **(b)** Training loss curves of models trained on various networks.

3,000 m. Overall, it can be concluded that the improved DT-LSTM algorithm had shorter running times and superior computational efficiency under different confidence levels and support degrees.

Figure 7 depicts the training accuracy curves of the proposed LSTM network and traditional CNN in this study. Figure 7a shows the training accuracy curves of different network models. After approximately 200 training steps, the accuracy of the proposed network rapidly improved and stabilized at around 0.9. Compared with the proposed network, the accuracy of traditional CNN improved more slowly and stabilized at a lower value, indicating that the convergence speed of the proposed network was faster and the accuracy was higher. Figure 7b shows the training loss curve, where the loss value of the proposed network rapidly decreased to near zero, while the loss of traditional CNN decreased more slowly and stabilized at a higher value. This indicated that the proposed network was more effective in improving accuracy and reducing losses during the training process, demonstrating superior training performance compared to traditional CNNs.

3.2 Analysis of life prediction results for NC machine tools

The improved DT-LSTM (the research method), traditional LSTM, PSO-SVM, and DT-ELM (Ensemble delta test - extreme learning machine) models were run separately on the test set, and relevant metrics were recorded. Table 2 presents the performance evaluation of existing methods and the research method, with evaluation metrics including Mean Absolute Error (MAE), Root Mean Square Error (RMSE), prediction accuracy, and the maximum deviation during the accelerated degradation phase. The experiment selected Transformer and CNN-LSTM as strong baselines. The Transformer model processed long sequence degradation data (such as 1800 h time series) through self attention mechanism, with a prediction accuracy of 91.5% (higher than traditional LSTM); The CNN-LSTM model extracted local features (such as high-frequency shock components of vibration signals) through CNN and captured temporal trends through LSTM. The MAE (15.7 h) was lower than traditional LSTM. The improved DT-LSTM model

TABLE 2 Performance evaluation of existing and research methods.

Model type	MAE/h	RMSE/h	Prediction accuracy/%	Maximum deviation during accelerated degradation stage/h
PSO-SVM	48.6	65.2	78.2	95
Traditional LSTM	32.4	45.8	85.9	62
DT-ELM	25.7	36.3	89.3	40
Transformer model	18.2	25.6	91.5	32
CNN-LSTM	15.7	21.3	92.8	28
Improved DT-LSTM	8.9	12.5	96.1	15

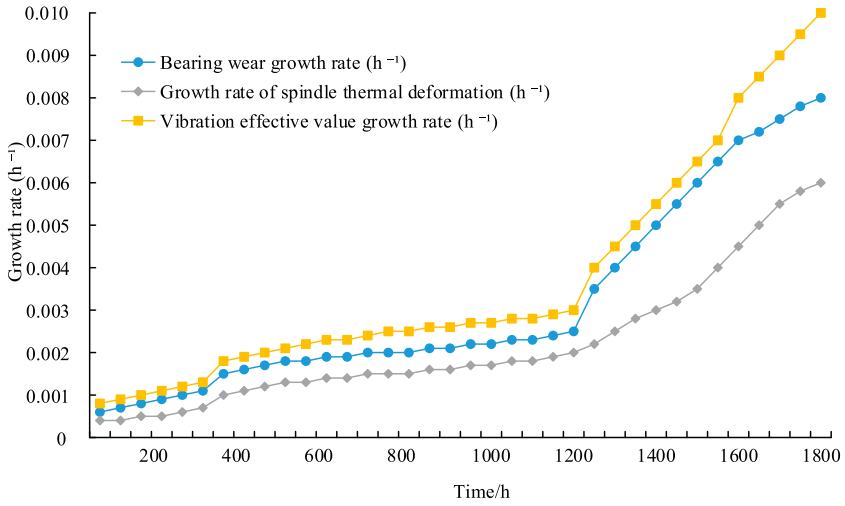

FIGURE 8
The process of standardized degradation index growth rate.

demonstrated the best performance across all core metrics: its prediction accuracy reached 96.1%, which was 10.2% higher than that of the traditional LSTM; its MAE was only 8.9 h, 81.7% lower than that of the PSO-SVM; and its maximum deviation during the accelerated degradation phase was merely 15 h. Meanwhile, it maintained a 100% compliance rate with physical constraints and a highly efficient prediction speed of 22 m, balancing accuracy, stability, and real-time performance, ensuring compatibility with the predictive maintenance demands specific to NC machine tools.

Figure 8 illustrates the growth rate process of standardized degradation indicators for the research model. It can be observed that all three types of indicators exhibited a phased increasing trend: from 50 to 300 h, it was the initial stable phase, with the lowest growth rates and gentle increases. Bearing wear rose from 0.0006 h^{-1} to 0.0011 h^{-1}, and the vibration effective value increased from 0.0008 h^{-1} to 0.0013 h^{-1}. From 300 to 1,200 h, the system entered a slow degradation phase, with steady increases in growth rates. Bearing wear reached 0.0025 h^{-1} (a 127% increase compared to 300 h), and the vibration effective value reached 0.003 h^{-1} (a 131% increase). After 1,200 h, the system entered an accelerated degradation phase, with a significant surge in growth rates. By 1800 h, bearing wear reached 0.008 h^{-1} (a 220% increase compared to 1,200 h), and the vibration effective value reached 0.01 h^{-1} (a 233% increase). Moreover, the growth rate of the vibration effective value consistently remained higher than those of bearing wear and spindle thermal deformation during the same periods, indicating that vibration signals were more sensitive to equipment degradation and could serve as a priority early warning indicator.

To confirm the superior performance of the introduced model, the comparison model was a basic model that did not incorporate physical constraints and an attention mechanism. The system proportion referred to the proportion of fusion between multi physics coupling data and actual monitoring data in the DT model, with a range of 0–1. The higher the ratio, the greater the proportion of physics coupling data in the fusion data. In Figure 9a, the comparison model (DT-LSTM) was selected as the standard benchmark. During the period of system proportion change, the precision, recall, and F0.5 indicators of the comparative model showed a gradually increasing trend, with lower peak values. For example, when the system proportion was 20%, the accuracy was about 18%. In Figure 9b, as the system proportion increased, the system proportion indicator of the model rapidly increased. When the system proportion reached 40%, the precision exceeded 40%, the

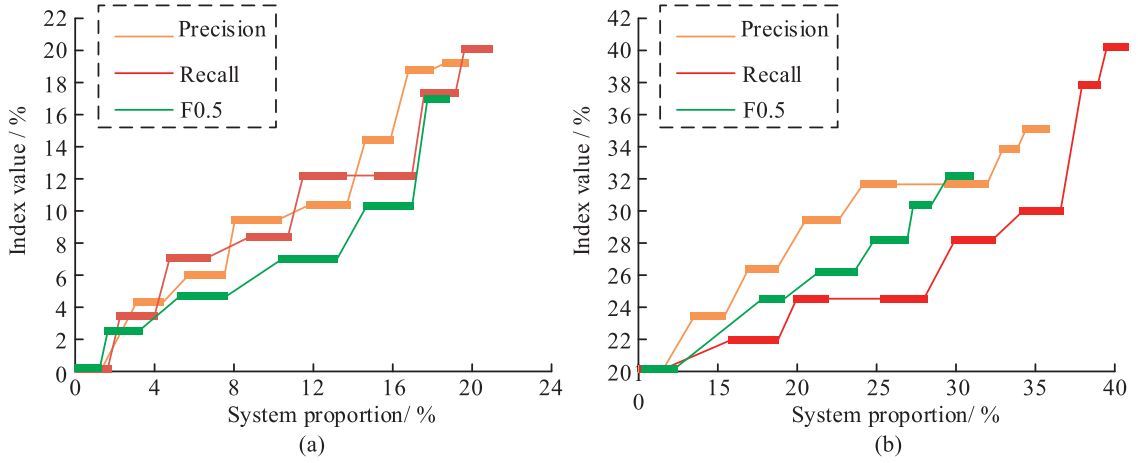

FIGURE 9
Accuracy, recall, and F0.5 metrics of different models in system proportion changes. **(a)** Comparison model. **(b)** Proposed model.

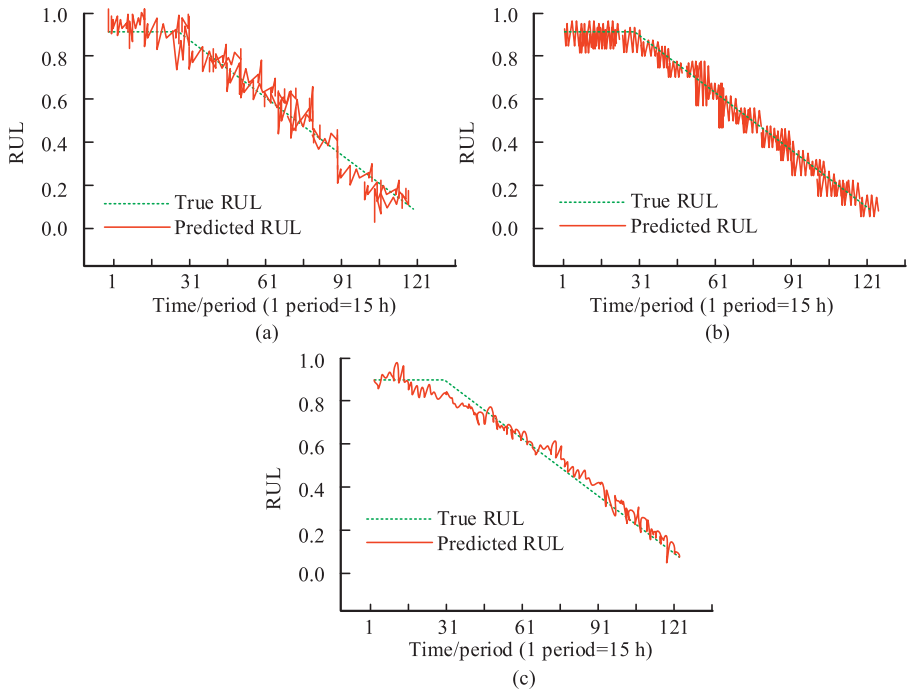

FIGURE 10
Comparison of RUL prediction results of different bearings. **(a)** Bearing 1. **(b)** Bearing 2. **(c)** Bearing 3.

recall rate approached 42%, and the F0.5 indicator also showed significant growth. The proposed model far exceeded the comparative model in terms of precision, recall ability, and overall evaluation. The proposed model exhibited stronger adaptability in data feature extraction and prediction.

Bearing1-3 all used the same acceleration degradation test conditions: speed of 8000r/min, radial load of 2000N, and ambient temperature of 35 °C. Figure 10 shows a comparison of predicted RUL results for different bearings, with the horizontal axis representing time (in Period (1 period = 15 h)) and the vertical axis representing RUL (where 0-1 represents the proportion of remaining life). In Figure 10a, the predicted RUL of Bearing 1 was similar to the true RUL trend in the early stages. In the later stage, due to increased bearing wear and noise interference, the predicted values showed greater fluctuations, with significant deviations between periods 91 and 121. In Figure 10b, the predicted RUL of Bearing 2 was usually very similar to the true value. Despite minor fluctuations, the model accurately tracked the true trend of lifespan decay, reflecting a certain degree of effectiveness. In Figure 10c, the predicted RUL of Bearing 3 was

slightly higher than the true value in the early stages, but gradually became consistent with the true value in the middle and late stages, indicating that the model had different adaptability to different degradation stages. Overall, the predictive model could roughly capture the decay pattern of bearing life.

The research model was validated based on the vertical machining center (VMC850), and its core advantage (multi physics coupling DT + physical constraint LSTM) had certain transferability, but key parameters needed to be adjusted according to the structural differences of different types of NC machine tools: NC lathe: compared with the vertical machining center, the main force on the lathe spindle was radial cutting force (the machining center is axial + radial composite force), and the boundary conditions of the force field module in the DT model needed to be adjusted, while modifying the attention weight of LSTM; NC milling machine: The feed system of the milling machine was a three-axis linkage, and a new "force vibration" coupling submodule for the feed axis needed to be added to the DT model to supplement the wear of the feed guide rail as a degradation feature, in order to avoid increasing generalization errors due to missing features; Longmen type machining center: Its large span (>2 m) led to uneven temperature field distribution. It was necessary to increase the number of temperature sensors in the DT model and optimize the boundary conditions of the heat conduction equation. Otherwise, the thermal deformation characteristic error of the LSTM input would increase by 15%–20%.

4 Discussion and conclusion

The study proposed a life prediction method for NC machine tools that integrates DT technology with an improved LSTM network. Specifically, a thermo-mechanical-vibration coupled DT model was constructed to achieve dynamic synchronization between the physical equipment and its virtual counterpart, enabling the extraction of multi-modal standardized degradation indicators. Subsequently, an attention mechanism and physical constraint regularization were introduced to develop an improved LSTM model for RUL prediction. Experimental findings demonstrated that the training accuracy curve of the proposed network rapidly increased and stabilized at around 0.9 after approximately 200 training steps. In contrast, the comparison network exhibited slower accuracy improvement and ultimately stabilized at a lower value, indicating faster convergence and higher accuracy in the proposed network. Regarding the training loss curve, the loss value of the proposed network quickly decreased to near zero, while the comparison network showed slower loss reduction and a higher final loss value. The improved DT-LSTM model outperformed other models across all core metrics: its prediction accuracy reached 96.1%, a 10.2% improvement over the traditional LSTM; its MAE was only 8.9 h, an 81.7% reduction compared to the PSO-SVM; and during the accelerated degradation phase, its maximum deviation was merely 15 h. Additionally, it maintained a 100% compliance rate with physical constraints and achieved an efficient prediction speed of 22 m, balancing accuracy, stability, and real-time performance to fully meet the predictive maintenance requirements of NC machine tools. It was evident that the improved LSTM model enhanced prediction accuracy and reliability for long-term degradation data through the incorporation of an attention mechanism and physical constraints. However, the study still had limitations. For instance, the multi-physics coupling calculations in the DT model relied on software with limited customization capabilities, restricting flexibility in model parameter adjustments. Future research directions can develop lightweight DT coupled simulation modules to reduce dependence on commercial software and improve parameter adjustment efficiency.

Data availability statement

The original contributions presented in the study are included in the article/supplementary material, further inquiries can be directed to the corresponding author.

Author contributions

JW: Conceptualization, Data curation, Formal Analysis, Investigation, Methodology, Writing – original draft, Writing – review and editing.

Funding

The author(s) declared that financial support was not received for this work and/or its publication.

Conflict of interest

The author(s) declared that this work was conducted in the absence of any commercial or financial relationships that could be construed as a potential conflict of interest.

Generative AI statement

The author(s) declared that generative AI was not used in the creation of this manuscript.

Any alternative text (alt text) provided alongside figures in this article has been generated by Frontiers with the support of artificial intelligence and reasonable efforts have been made to ensure accuracy, including review by the authors wherever possible. If you identify any issues, please contact us.

Publisher's note

References

Dimic, Z., Zivanovic, S., Pavlovic, D., Furtula, M., Djurkovic, M., Rakic, A., et al. (2024). Reconfigurable open architecture control system with integrated digital twin for 3-axis woodworking milling machine. *Wood Material Science & Engineering* 19 (1/6), 1295–1304. doi:10.1080/17480272.2024.2318024

Gao, B., Ye, Y., and Pan, S. H. Y. (2023). A dynamic reliability prognosis method for reusable spacecraft mission planning based on digital twin Framework.ASCE-ASME journal of risk and uncertainty in engineering systems, part B. *Mech. Eng.* 9 (4), 1–9. doi:10.1115/1.4063297

Hu, F., Zou, X., Hao, H., Hou, P., and Huang, Y. (2024). Research and application of simulation and optimization for CNC machine tool machining process under data semantic model reconstruction. *Int. J. Adv. Manuf. Technol.* 132 (1), 801–819. doi:10.1007/s00170-024-13415-z

Information, V. F. A., Cole, C., Information, V. F. A., Spiryagin, M., Information, V. F. A., Wu, Q., et al. (2024). Augmented digital twin for railway systems. *Veh. Syst. Dyn. Int. J. Veh. Mech. Mobil.* 62 (1), 67–83. doi:10.1080/00423114.2023.2194543

Kibira, D., Shao, G., Venketesh, R., and Triebe, M. J. (2024). Building a digital twin of a CNC machine tool. *Winter Simul. Conf. (WSC)* 1 (1), 2915–2926. doi:10.1109/wsc63780.2024.10838819

Kombarov, V., Fojtu, P., Sulitka, M., Aksonov, Y., Sveda, J., Tsegelnyk, Y., et al. (2025). Prediction and compensation of motion differential characteristics influence on position error in CNC machine tools. *Int. J. Adv. Manuf. Technol.* 137 (11), 5951–5981. doi:10.1007/s00170-025-15510-1

Norberger, M., Rehm, M., Schlegel, H., Dix, M., and Patalas-Maliszewska, J. (2024). Review of methods for developing and integration of a digital twin in NC-based production systems. *IFAC-PapersOnLine* 58 (19), 1012–1017. doi:10.1016/J.IFACOL.2024.09.143

Pantelidakis, M., and Mykoniatis, K. (2024). Extending the digital twin ecosystem: a real-time digital twin of a LinuxCNC-controlled subtractive manufacturing machine. *J. Manuf. Syst.* 74 (1), 1057–1066. doi:10.1016/j.jmsy.2024.05.012

Pei, F., Chen, S., Li, Q., Guo, S., Xi, Y., and Huang, P. (2025). Construction method of CNC machine tool digital twin model based on the four-layer framework. *IEEE Access* 13 (1), 70211–70227. doi:10.1109/ACCESS.2025.3560647

Peterson, L., Gosea, I. V., Benner, P., and Sundmacher, K. (2025). Digital twins in process engineering: an overview on computational and numerical methods. *Comput. & Chem. Eng.* 193 (2), 1–108917.21. doi:10.1016/j.compchemeng.2024.108917

Preethi, P., and Mamatha, H. R. (2023). Region-based convolutional neural network for segmenting text in epigraphical images. *Artif. Intell. Appl.* 1 (2), 119–127. doi:10.47852/bonviewAIA2202293

Qu, H., Chen, J., and Cai, Y. (2025). A digital twin approach for weld penetration prediction of tig welding with dual ellipsoid heat source. *J. Intelligent Manuf.* 36 (6), 4083–4103. doi:10.1007/s10845-024-02431-1

Sa, G., Jiang, Z., Liu, Z., Liu, Z., Sun, J., Qiu, C., et al. (2024a). An integrated optimization method for measurement points layout and error modeling for digital twin of CNC machine tools. *Precis. Eng.* 90 (1), 1–11. doi:10.1016/j.precisioneng.2024.07.013

Sa, G., Sun, J., Hou, M., Jiang, Z., Liu, Z., Mao, H., et al. (2024b). A digital twin synchronous evolution method of CNC machine tools associated with dynamic and static errors. *Int. J. Adv. Manuf. Technol.* 134 (5), 2753–2763. doi:10.1007/s00170-024-14244-w

Tao, F., Liu, A., Anwer, N., Zhang, M., Wang, L., and Nee, A. Y. C. (2024). Editorial for the special issue on digital twin in industry. *Int. J. Adv. Manuf. Technol.* 131 (11), 5365–5367. doi:10.1007/s00170-024-13440-y

Uribe, D., Baudouin, C., Durand, C. B. R., and Bigot, R. (2024). Predictive control for a single-blow cold upsetting using surrogate modeling for a digital twin. *Int. J. Material Form. Official J. Eur. Sci. Assoc.* 17 (1), 7–12. doi:10.1007/s12289-023-01803-x

Wang, L., Liang, H., Tang, Y., Mao, G., Zhang, H., and Zhao, D. (2024). DRL-based joint resource allocation and platoon control optimization for UAV-hosted platoon digital twin. *IEEE Internet Things Journal* 11 (22), 37114–37126. doi:10.1109/JIOT.2024.3439576

Wei, Y., Hu, T., Yue, P., Luo, W., and Ma, S. (2024). Study on the construction theory of digital twin mechanism model for mechatronics equipment. *Int. J. Adv. Manuf. Technol.* 131 (11), 5383–5401. doi:10.1007/s00170-022-09144-w

Xie, X., Zhang, X., Sun, Z., Song, Y., and Huang, H. (2024). Digital twin experimental platform for the parameter design of a servo system of computer numerical control machine tools. *Exp. Technol. Manag.* 41 (5), 113–120. doi:10.16791/j.cnki.sjg.2024.05.016

Zohdi, T. I. (2025). A voxel-based machine-learning digital-oven-twin for precise cooking. *Comput. Mech.* 75 (5), 1501–1518. doi:10.1007/s00466-024-02575-0